Recent Development on surface-textured ZnO:Al Films prepared by Sputtering for Thin-Film Solar Cell Application

M. Berginski[a)], J. Hüpkes[a)], W. Reetz[a)], B. Rech[a),b)], M. Wuttig[c)]

[a)] Institute of Photovoltaics (IEF-5), Forschungszentrum Jülich GmbH, D-52425 Jülich, Germany, Tel: +49 2461 61 3242, Fax: +49 2461 61 3735, e-mail: M.Berginski@fz-juelich.de

[b)] Department of Silicon Photovoltaics (SE 1), Hahn-Meitner-Institut Berlin GmbH, D-12489 Berlin, Germany

[c)] Institute of Physics (IA), RWTH Aachen University, D-52056 Aachen, Germany

Abstract

This study addresses the optimization of magnetron-sputtered aluminum-doped zinc oxide (ZnO:Al) thin films as front contact in silicon thin-film solar cells. The front contact has to be highly conductive and highly transparent for the visible as well as for the infrared spectrum. Furthermore, it has to scatter the incident light efficiently leading to an effective light trapping inside the silicon layers. To materialize the scattering phenomenon, the surface of the magnetron-sputtered ZnO:Al thin films are textured by wet-chemical etching. In this contribution we focus on an optimized balance between electrical and optical needs maintaining a surface topography well suited for light trapping. In a first step we study the influence of vacuum annealing on ZnO:Al films on glass substrates. An increase in transmission is observed while the carrier concentration is gradually decreased. Application of vacuum-annealed ZnO:Al films in silicon thin-film solar cells allows the determination of the relationship between the front-contact carrier concentration and the short-circuit current density. Also, an optimized carrier concentration for the solar module application has been estimated. In a second step we apply this knowledge for direct fabrication of ZnO:Al layers with optimized carrier

concentration by varying the target doping concentration (TDC). Nevertheless, changing the TDC alters the ZnO:Al properties and especially the texturing behavior of the thin films as well. Thus, we present a parameter study of TDC and substrate temperature during sputtering to prepare front contacts with surface topography enabling efficient light trapping and ideally balancing optical and electrical properties for solar module applications.

Keywords : thin-film solar cells, light trapping, zinc oxide, vacuum annealing

Introduction

Silicon thin-film solar cells are promising candidates for photovoltaic power generation in future [1],[2]. The most advanced approach employs hydrogenated amorphous (a-Si:H) and microcrystalline silicon (µc-Si:H) as active layers in single or multi-junction cells [3]-[6]. Silicon thin-film solar cells in the p–i–n (superstrate) configuration require a transparent conductive oxide (TCO) film as front contact, which has to combine low series resistance and high transparency in the visible (400 nm to 800 nm) and, for µc-Si:H based cells, also in the near infrared (NIR) spectral range (up to 1100 nm). Furthermore, an adapted surface topography is required to provide light scattering and subsequent light trapping inside the silicon solar cell structure. Optimization of the front-contact TCO has proven to be crucial for a high cell efficiency [7].

Radio frequency (rf) sputter-deposited aluminum-doped zinc oxide (ZnO:Al) thin film is a promising candidate as front-contact TCO. In a preceding work Agashe et al. studied the influence of the target doping concentration (TDC) on the electrical and optical properties of sputter-deposited ZnO:Al films [8]. Much lower parasitic absorptions were found in the work with only slightly reduced conductivity values using sputter targets with low amount of alumina. These sputter-deposited ZnO:Al thin films are optically smooth and, thus, do not scatter the light. By wet-chemical etching the sputtered ZnO:Al films become rough and can introduce light

scattering and subsequent light trapping in thin-film solar cells [9]-[11]. Kluth et al. related the influence of pressure and substrate temperature during sputter deposition of ZnO:Al to structural properties and post-etching surface topography [11]. The surface topography determines the light-trapping ability to a large extent. In general, TCO transmission, conductivity and post-etching surface topography are interrelated with each other. Hence, the tailoring of all film properties for solar cell applications is a highly challenging task.

In this work we focus on an optimized balance between electrical and optical properties of ZnO:Al thin films with a surface topography that is well suited for light trapping. We first concentrate on texture-etched and vacuum-annealed ZnO:Al. The post-etching annealing step decreases the free-carrier concentration although maintains the desired surface topography. This allows the study of the relationship between TCO transmission and cell current density experimentally. The calculations for electrical and dead-area losses in module applications were employed to identify an optimized range of ZnO:Al carrier concentration which provides the highest module efficiency.

In a second step we prepared front-contact ZnO:Al thin films with optimally balanced electro-optical properties directly without post-etching vacuum-annealing step. For this reason, the TDC was varied. It was found that the substrate temperature during sputtering had to be adapted in order to maintain post-etching surface topographies efficient for light trapping.

Experimental

The ZnO:Al films were prepared on Corning 1737 glass with substrate size of 10x10 cm^2 by rf-magnetron sputtering from ceramic targets with 0.2, 0.5, or 1 wt% Al_2O_3 content. The target doping concentration is henceforth referred to as TDC. At constant deposition pressure of 0.1 Pa and 0.3 Pa, respectively, the substrate temperature was varied in a range of 60 – 490 °C. The substrate temperature was calibrated by a thermal sensor and was controlled by the heater temperature. The typical 900 nm thick smooth ZnO:Al films (root mean square (rms) roughness

about 15 nm) were surface-textured by wet-chemical etching with diluted hydrochloric acid (0.5% HCl). This leads to a rms roughness of higher than 100 nm. To study the relationship between ZnO:Al transmission and solar cell short-circuit current density, the samples were prepared using a TDC of 1 wt% at substrate temperature of 300 °C. These substrates were cut into two pieces after surface texturing. One piece of each sample was annealed in vacuum (pressure lower than 10^{-4} Pa) at substrate temperatures T_S = 300°C to 500 °C, while the other half remained untreated and served as a reference. Samples with gradually varied properties were fabricated by using different annealing temperatures and durations of annealing as well as several annealing cycles. The characterization of electrical properties was performed by four-point probe and room temperature Hall effect measurements in van der Pauw geometry. The relative measurement error for carrier concentration and mobility was ±5% and for the sheet resistance ±2%, respectively. The optical transmittance and reflectance were measured in air with a dual-beam spectrometer where for an exact measurement of rough TCO films, CH_2I_2 was applied as index-matching fluid to avoid systematic measurement errors due to light scattering and internal light trapping [12]. The measurement error for these optical data (T and R) was smaller than ±3%. The surface topography and its characteristic feature size were studied by scanning electron microscopy (SEM) and atomic force microscopy (AFM). The AFM data were evaluated to determine the rms roughness. The light-trapping ability of a specific TCO film was evaluated by the application in solar cells. The silicon layers were prepared using plasma-enhanced chemical vapor deposition (PECVD) at 13.56 MHz excitation frequency in a 30x30 cm^2 reactor. The details of this process, the PECVD system and cell preparation have been described elsewhere [13],[14]. The double layers of sputter-deposited ZnO:Al (80 nm) and thermally evaporated silver (700 nm) served as back reflector and rear-side contact. The solar cell I/V-characteristics were measured using a solar simulator (Wacom WXS-140S-Super) at standard test conditions (AM 1.5, 100 mW/cm², 25 °C). The external quantum efficiency (QE) of the solar cells was calculated from spectral response measured at zero bias. The integrated short-

circuit current density was calculated from the QE curve employing the AM 1.5 solar spectrum. Henceforth this calculated current density is referred to as cell current density j_{QE}. The spectral response measurements were highly reproducible. Thus, the calculated cell current density j_{QE} exhibited a measurement reproducibility error of only ±1%.

Results

1. Balancing optical and electrical ZnO:Al properties

1.1. Vacuum annealing of ZnO:Al

The effect of vacuum annealing on the electrical and optical properties of ZnO:Al front contacts was investigated. While for example Tsuji et al. and Fang et al. [15],[16] reported a decrease of resistivity upon vacuum annealing of sputter-deposited ZnO:Al films, other authors – for example Haug et al. [17] – found an increase in resistivity due to a decrease of carrier concentration. Fig. 1 shows experimental results of as-deposited smooth ZnO:Al films after vacuum annealing for one hour at various temperatures. The TDCs of 0.2 wt% (circles) and 1 wt% (squares) were applied for sputter deposition at two different substrate temperatures (see inset of Fig. 1). The sheet resistance R_{sheet} (Fig. 1a) can be reduced by vacuum annealing at temperatures below 400 °C in case of T_S = 65 °C. X-ray diffraction spectra in Bragg-Brentano geometry revealed healing of stress by shift of (002)-peak position and shrink of (002)-peak width (not shown). This effect leads to both higher mobility and higher carrier-concentration values. However, the mobility of these samples deposited at T_S = 65 °C is lower than its higher T_S counterpart. In contrast, films deposited at higher substrate temperatures (closed symbols) already have very high mobility in the initial case. Upon vacuum annealing the electrical properties of these layers remained constant up to annealing temperatures of 400 °C – 500 °C. For all films annealing at temperatures up to 600 °C leads to a decrease of carrier concentration. In conclusion, resistivity of low-quality ZnO:Al films especially with low crystalline quality can be decreased by vacuum annealing. Above a certain temperature the opposite is the case: the

strong drop of carrier concentration leads to an increase of resistivity. It is interesting to note, that the mobility of high quality ZnO:Al films remains at rather high level. In the following experiments we utilized these features in order to study the influence of the interrelated properties transparency and carrier concentration on the performance of silicon thin-film solar cells. ZnO:Al films deposited using a TDC of 1 wt% and T_S = 300 °C were used for this purpose, since they exhibit very low sheet resistance and high carrier mobility in the initial state. The transmission and absorption data of surface-textured ZnO:Al thin films before and after vacuum annealing are compared in Fig. 2(a). The transmission in the long wavelength part of the spectrum increased with heat treatment gradually. At the same time the absorption decreases due to a shift of the free-carrier absorption towards longer wavelengths and a reduction in absorption-peak height [18]. As indicated in Fig. 2 the sheet resistance R_{sheet} increases upon vacuum annealing.

The Hall measurement results are shown in Fig. 2(b). The carrier concentrations of untreated ZnO:Al samples vary in the range of 4.1×10^{20} cm^{-3} to 4.8×10^{20} cm^{-3}. By longer vacuum annealing or annealing at higher temperatures the carrier concentration is irreversibly and gradually reduced down to 1.5×10^{20} cm^{-3}. The mobility remains in the range of 42 cm^2/Vs to 48 cm^2/Vs. Consequently, the resistivity of the ZnO:Al thin films increased from 3×10^{-4} Ωcm to 1×10^{-3} Ωcm (not shown) and the sheet resistance increased from 4 Ω to 12 Ω. The thickness *d* of the films did not change within the measurement accuracy of ±15 nm for these films with a peak to peak roughness of more than 300 nm.

For application in µc-Si:H solar cells the surface topography of the TCO is very crucial. In order to investigate the influence of the vacuum annealing on the surface topography, we applied SEM and AFM measurements and compared the surface topography of untreated and vacuum-annealed ZnO:Al films. The AFM data was analyzed statistically. The heat treatment does not alter the surface topography noticeably (for details see [19]).

1.2. Application in µc-Si:H single-junction solar cells

The quantum efficiency of solar cells is expected to increase with the increase in transmission of the front TCO. The vacuum-annealed front contacts shown in Fig. 2 were applied in identical µc-Si:H single-junction cells. Fig. 3 shows QE data and total cell absorption 1-R_{cell} (cell reflection R_{cell}) of solar cells prepared on the ZnO:Al films shown in Fig. 2. Without any heat treatment of the front contacts the cell current density, calculated employing the QE data, is 22.3 mA/cm^2. The treatment of the ZnO:Al films increases the quantum efficiency of the solar cells in the wavelength range $\lambda > 500$ nm. A small shift in QE occurs at wavelength $\lambda \approx 350$ nm due to the Burstein-Moss effect of the ZnO:Al with different carrier concentration [20],[21]. Additionally, in the short-wavelength range ($\lambda < 500$ nm) small variations are caused by absorption losses in the very thin boron-doped silicon p-layer due to small differences in thickness. This might influence the cell current density by less than 0.3 mA/cm^2. An improvement of cell current density by 1.3 mA/cm^2 is achieved, which is caused by the vacuum annealing of the front-contact ZnO:Al. The cell current density can be raised up to 23.6 mA/cm^2, a very high value considering, that the thickness of the µc-Si:H absorber layer is only 0.9 µm. At the same time the total cell absorption 1-R_{cell} was decreased in the long wavelength range since parasitic absorption losses in the TCO were reduced. This is completely attributed to an increase in front-contact transmission (compare Fig. 2). An alternative explanation could be an improved light injection and scattering into the active silicon layers due to changes in the refractive index with reduced carrier-concentration value. However, we expect only a minor change in the refractive index (λ = 500−1100 nm) for the limited range of carrier concentrations studied here [22].

Fig. 4 evaluates the data of all solar cells deposited in this study. The cell current density is plotted versus carrier concentration N of the corresponding front-contact TCO. The line represents a cubic fit of the cell data. Since the TCO absorption is directly related to N and since the TCO surface topography is maintained, Fig. 4 gives an experimental correlation between the carrier concentration in the front contact and the cell current density of a microcrystalline-silicon

solar cell.

1.3 Calculations for module applications

The conversion efficiency of solar cells and modules is limited by both optical and electrical losses. Even though the cell current density can be increased by heat treatment of front-contact TCO, increased Ohmic loss due to increase in front-contact resistance have to be considered. In module applications the active cell area consists of cell stripes (active width w_a) that are separated e.g. by laser scribing. Decreasing the active cell width decreases the influence of TCO-conductivity on the module efficiency on the expense of higher dead-area loss. According to a model by Gupta et al. efficiencies of solar modules have been calculated from real maximum power point values of current density J_{MPP} and voltage V_{MPP} including the effect of Ohmic loss in the TCO and area loss by cell interconnection [23]. The expected aperture area efficiency η_{ap} is calculated by:

$$\eta_{ap} = \frac{J_{MPP} V_{MPP} (1 - f)}{P_{ls}} \tag{1}$$

with power density P_{ls} of the light source and Ohmic and dead-area losses f given by:

$$f = \frac{w_d}{w_a + w_d} + \frac{J_{MPP}}{V_{MPP}} \frac{R_{sheet}}{3} \frac{w_a^3}{w_a + w_d}. \tag{2}$$

The dead-area width w_d was assumed to be 300 µm and the TCO sheet resistance R_{sheet} was determined in Hall measurements (see Fig. 2(b)). The optimum active cell width $w_{a,opt}$ was calculated using the approximation $w_a + w_d \approx w_a$ by:

$$w_{a,opt} = \sqrt[3]{\frac{3}{2} \frac{V_{MPP}}{J_{MPP}} \frac{w_d}{R_{sheet}}}. \tag{3}$$

The single-junction µc-Si:H solar modules are discussed in the following. Measured values V_{MPP} of 1x1 cm^2 sized single-junction µc-Si:H solar cells were used for the calculations. V_{MPP} varied in the range of 0.38 V to 0.41 V. In case of untreated front contacts the correspondingly measured

J_{MPP} values were used (mean value of reference cells: $J_{MPP,mean}$ = 20.4 mA/cm^2). The gain in cell current density of solar cells with vacuum-annealed front contacts was incorporated into the calculations by relative change of J_{MPP} employing the experimental cell current density data j_{QE}. The values of $w_{a,opt}$ vary between 4 mm and 6 mm in case of front-contact carrier concentration in the range of 1.5x10^{20} cm^{-3} to 4.3x10^{20} cm^{-3}. The aperture area efficiency η_{ap} of a single-junction µc-Si:H solar module was calculated employing equations (2) and (1) and constant w_a = 5 mm. Normalized aperture-area module efficiencies with respect to calculations based on averaged reference cell data are given in Fig. 4 (right axis, hexagonal points). In order to get an idea about the general trend, cubic fits for j_{QE} (Fig. 4, solid line) and R_{sheet} (compare Fig. 2(b)) versus carrier concentration and constant V_{MPP} (average value of 1x1 cm^2 cell measurements) were used for additional calculations and are shown as lines in Fig. 4. The two cases of considering an optimal cell width $w_{a,opt}$ (dotted line) and a constant cell width of w_a = 5 mm (dashed line) in the calculation of η_{ap} are shown. For both cases η_{ap} is maximal at carrier concentrations in the range of 2.1x10^{20} cm^{-3} to 2.4x10^{20} cm^{-3}. As a result of these calculations, an increase in aperture-area module efficiency of up to 3.5% relative is expected by using the front contact with optimized carrier concentration as compared to an untreated front contact with N = 4.4x10^{20} cm^{-3}.

In contrast to single-junction µc-Si:H modules as discussed so far, in case of a multi-junction solar modules Ohmic loss is less relevant, because these modules operate at higher voltages V_{MPP} and lower currents J_{MPP} (due to series interconnection of the junctions). This criteria shifts the optimized carrier concentration value towards slightly lower values and thereby realization of a gain in efficiency is even more significant for multi-junction device structure, using an optimally balanced front ZnO:Al.

The module efficiency of silicon thin-film solar-cell devices is strongly dependent on the detailed characteristic of the light-trapping ability. Thus, the result of the optimization of the carrier concentration presented here is only applicable in case of wet-chemically textured magnetron-sputtered ZnO:Al films with post-etching surface topography consisting of quite regularly

distributed craters with mean opening angles between 120° and 135° and lateral sizes of 1 to 3 µm. A carrier concentration below $3x10^{20}$ cm^{-3} is usually found in case of ZnO:B films for application in silicon thin-film solar cells deposited by low-pressure chemical vapor deposition (LP-CVD) with a thickness of 2 µm to 6 µm [24]. Inthis respect, those films might be favorable for this application. However, direct transfer of our optimized carrier-concentration value estimation is difficult, due to the importance of light scattering (ZnO:B thin films develop a different kind of surface topography during growth) and the utilized input parameters for calculations extracted experimentally from application of ZnO:Al films with a thickness below 1 µm.

2 Variation of target doping concentration

Another way to control the carrier-concentration value in ZnO:Al is a variation of the doping concentration. A reduced TDC leads to lower N and also high μ is possible [8],[25]. From previous work it is known, that the substrate temperature has a strong impact on the electrical properties [26],[27]. Thus, we investigated the influence of the substrate temperature on ZnO:Al film properties for different target doping concentration. For each series all other deposition parameters were kept constant. Fig. 5 (a) represents the carrier concentration as function of substrate temperature T_S for different TDC. A carrier concentration in the range of $2.0x10^{20}$ cm^{-3} to $2.5x10^{20}$ cm^{-3} can be realized employing a TDC of 1 wt% and T_S = 70°C or a TDC of 0.5 wt% and T_S= 460°, respectively.

In case of vacuum annealing the carrier mobility remains constant within ±7%. Hence the resistivity and sheet resistance mainly depends on the carrier concentration. However, in case of varying TDC and substrate temperature, the carrier mobility is not constant. Fig. 5 (b) plots the resistivity of the films against substrate temperature for various values of TDC. In general, the lowest resistivity values are found in case of TDC 1 wt%. However, at substrate temperature of 350 °C the resistivity of ZnO:Al films sputtered using a TDC of 0.5 wt% were comparable low.

Fig. 5(c) shows the current densities j_{QE} of single-junction µc-Si:H solar cells with an intrinsic silicon absorber layer thickness of 1 µm deposited on these ZnO:Al films. The highest cell current densities with a peak value of 24.4 mA/cm^2 are found for a TDC of 0.5 wt% at substrate-temperature range between 350 °C and 380 °C, and also for a TDC of 0.2 wt% at substrate temperature of 415 °C. For these parameters the cell current density is even higher than in case of vacuum annealing as discussed in the first part of this work. About 0.4 mA/cm^2 can be attributed to the slightly larger i-layer thickness.

A comparison of the carrier concentration (Fig. 5a) and the cell current densities (Fig. 5c) clearly shows that the cell current densities are not maximized in case of overall lowest N (TDC 0.2 wt%, low substrate temperature). The low carrier concentration and high cell current density are not directly related to each other any more, because the texturing behavior (determining the light-trapping ability) depends also on the deposition parameters.

A detailed study of the texturing behavior has shown, that only for substrate temperatures between two transition temperatures the post-etching surface topography consists of regularly distributed craters with mean opening angles between 120° and 135° and lateral sizes of 1 to 3 µm [27]. This kind of surface topography enables very efficient light trapping. The transition temperatures shift to higher values with decreasing TDC. While in case of a TDC of 1 wt% the substrate-temperature range is 270 °C to 400 °C, for a TDC of 0.2 wt% the substrate temperature should be above 400 °C.

Thus, Fig. 5(c) shows that in case of TDC 0.5 wt% and substrate temperature in the range of 350 °C to 380 °C and for a TDC of 0.2 wt% and substrate temperature of 415 °C the convolution of the two properties transmission and light scattering results in maximized cell current density. Among these parameter pairs a TDC of 0.5 wt% shows significantly better electrical properties. The resistivity is as low as 0.4x10^{-3} Ωcm. In case of vacuum annealing the optimally balanced conductivity was 0.7x10^{-3} Ωcm. Thus, at a TDC of 0.5 wt% and $T_S \approx 360$ °C both a higher cell current density and a higher conductivity than in case of vacuum annealing and optimally

balanced electro-optical properties are found. This deposition regime is especially promising for high-efficiency module application.

Conclusions

The vacuum annealing of ZnO:Al films was investigated for various deposition conditions. The ZnO:Al films sputtered at a low substrate temperature show comparatively low mobility. Upon vacuum annealing, the electrical properties can be enhanced. In case of as-deposited high-quality ZnO:Al films, vacuum annealing at temperatures above 500 °C for one hour significantly decreases the carrier concentration.

Applying vacuum annealing after front-contact wet-chemical texture etching and before silicon deposition favors optical properties: the transmission is increased due to reduced free-carrier absorption. While the surface topography and the carrier mobility remain unaltered, the resistivity increases. Application of the gradual treatment of front contacts in µc-Si:H single-junction cells allows the study of the relationship between the cell current density and sheet resistance for a given and constant front-contact surface topography. These results were utilized to calculate solar module efficiency. The module efficiency is expected to be increased by more than 3.5% relative by optimally balanced electrical and optical front-contact properties. The carrier concentrations are in the range of 2.0×10^{20} cm^{-3} to 2.5×10^{20} cm^{-3} and are expected to be the optimum for these types of modules in case of high (> 40 cm^2/Vs) carrier mobility.

In a second step front contacts with balanced optical and electrical properties were deposited directly without any post-etching treatment step by variation of the target doping concentration and the substrate temperature. A study in single-junction µc-Si:H solar cells has identified a target doping concentration of 0.5 wt% (Al_2O_3 in ZnO) and a substrate-temperature range of 350 °C to 380 °C as very promising deposition parameter space for higher module efficiency.

Acknowledgements

The authors would like to thank A. Doumit, J. Kirchhoff, J. Klomfaß, G. Schöpe, and H. Siekmann for technical assistance, and C. Das and S. Haas for helpful discussions. We gratefully acknowledge financial support from the Bundesministerium für Umwelt, Naturschutz und Reaktorsicherheit (German Federal Ministry for the Environment, Nature Conservation and Nuclear Safety) (contract no. 0329923 A) and the European Commission (Athlet project, contract no. 019670).

References

[1] S. Hegedus, Prog. Photovolt: Res. Appl. 14 (2006) 393.

[2] M.A. Green, Prog. Photovolt: Res. Appl. 14 (2006) 383.

[3] J. Meier, U. Kroll, T. Roschek, J. Spitznagel, S. Benagli, C. Ellert, G. Androutsopoulos, A. Hügli, W. Stein, J. Springer, O. Kluth, D. Borello, M. Poppeller, G. Büchel, A. Büchel, Proceedings of the 15th International Photovoltaic Science & Engineering Conference, Shanghai, China, October 10-15, 2005, p. 238.

[4] B. Rech, T. Repmann, S. Wieder, M. Ruske, U. Stephan, Thin Solid Films 502 (2006) 300.

[5] S. Wieder, M. Liehr, T. Repmann, B. Rech, Proceedings of the 15th International Photovoltaic Science & Engineering Conference, Shanghai, China, October 10-15, 2005, p. 145.

[6] K. Yamamoto, A. Nakajima, M. Yoshimi, T. Sawada, S. Fukuda, T. Suezaki, M. Ichikawa, Y. Koi, M. Goto, T. Meguro, T. Matsuda, M. Kondo, T. Sasaki, Y. Tawada, Proceedings of the 15th International Photovoltaic Science & Engineering Conference, Shanghai, China, October 10-15, 2005, p. 529.

[7] B. Rech, H. Wagner, Appl. Phys. A 69 (1999) 155.

[8] C. Agashe, O. Kluth, J. Hüpkes, U. Zastrow, B. Rech, J. Appl. Phys. 95 (2004) 1911.

[9] F. C. M. van de Pol, F. R. Blom Th. J. A. Popma, Thin Solid Films 204 (1991) 349.

[10] O. Kluth, B. Rech, L. Houben, S. Wieder, G. Schöpe. C. Beneking, H. Wagner, A. Löffl, H. W. Schock, Thin Solid Films 351 (1999) 247.

[11] O. Kluth, G. Schöpe, J. Hüpkes, C. Agashe, J. Müller, B. Rech, Thin Solid Films 442 (2003) 80.

[12] Y. Gotoh, A. Adachi, M. Mizuhashi, Reports Res. Lab. Asahi Glass Co., Ltd., 37 [1] (1987) 13 (in Japanese); similar: M. Mizuhashi, Y. Gotoh, K. Adachi, Jap. J. Appl. Phys. 27 (1988) 2053.

[13] B. Rech, T. Roschek, T. Repmann, J. Müller, R. Schmitz, W. Appenzeller, Thin Solid Films 427 (2003) 157.

[14] B. Rech, T. Repmann, M.N. van den Donker, M. Berginski, T. Kilper, J. Hüpkes, S. Calnan, H. Stiebig, S. Wieder, Thin Solid Films 511-512 (2006) 548.

[15] T. Tsuji, M. Hirohashi, Appl. Surf. Science, 157 (2000) 47.

[16] G. J. Fang, D. Li, B.-L. Yao, Thin Solid Films, 418 (2002) 156.

[17] F.-J. Haug, Zs. Geller, H. Zoog, A. N. Tiwari, C. Vignali, J. Vacuum Science Technol. A, 19 (2001) 171.

[18] T. J. Coutts, D. L. Young, X. Li, MRS-Bulletin: Transparent Conducting Oxides 25 (2000) 58.

[19] M. Berginski, B. Rech, J. Hüpkes, G. Schöpe, M.N. van den Donker, W. Reetz, T. Kilper, M. Wuttig, in: J. Poortmans, H. Ossenbrink, E. Dunlop, P. Helm (Eds.), Proceedings of the 21st European Photovoltaic Solar Energy Conference, Dresden, Germany, September 4-8, 2006, p. 1539.

[20] E. Burstein, Phys. Rev. 93 (1954) 632.

[21] T. S. Moss, Proc. Phys. Soc. London, Sect. B 67 (1954) 775.

[22] Z. Qiao, C. Agashe, D. Mergel, Thin Solid Films 496 (2006) 520.

[23] Y. Gupta, H. Liers, S. Woods, S. Young, R. DeBlasio, L. Mrig, Proceedings of the 16th IEEE Photovoltaic Specialists Conference, San Diego, California, September 27-30, 1982, p. 1092.

[24] J. Steinhauser, L. Feitknecht, S. Faÿ, R. Schlüchter, J. Springer, A. Shah, C. Ballif, in: W. Palz, H. Ossenbrink, P. Helm (Eds.), Proceedings of the 20th European Photovoltaic Solar Energy Conference, Barcelona, Spain, June 6-10, 2005, p. 1608.

[25] K. Ellmer, J. Phys. D: Appl. Phys., 34 (2001) 3097.

[26] J. Hüpkes, B. Rech, S. Calnan, O. Kluth, U. Zastrow, H. Siekmann, M. Wuttig, Thin Solid Films 502 (2006) 286.

[27] M. Berginski, J. Hüpkes, M. Schulte, G. Schöpe, H. Stiebig, B. Rech, M. Wuttig, J. Appl. Phys. 101 (2007) 74903.

List of figure captions

Fig. 1: Hall data (sheet resistance R_{sheet}, mobility μ and carrier concentration N) of smooth ZnO:Al films before (data on the left, denoted by 'ref.') and after vacuum annealing for 1 hour at various temperatures up to 600 °C. The ZnO:Al films were sputtered using a TDC of 1 wt% (squares) and of 0.2 wt% (circles), respectively. The closed and open symbols represent high and low substrate temperature T_S during deposition, respectively (see inset).

Fig. 2: Optical (top) and electrical (bottom) properties of texture-etched ZnO:Al front contacts. Transmission T and absorption A=1-T-R spectra of samples before (full lines) and after vacuum annealing (broken lines) are shown in Fig 2(a). As electrical properties sheet resistance R_{sheet} (left axis Fig. 2(b), squares) and carrier mobility μ (right axis Fig. 2(b), triangles) are plotted against carrier concentration N. Data are shown of samples before (open symbols) and after (full symbols) vacuum annealing. The line represents calculated sheet-resistance values employing mean values of mobility (μ_{mean} = 44.7 cm^2/Vs) and film thickness (d_{mean} = 797 nm), respectively.

Fig. 3: Quantum efficiency QE and total cell absorption 1-R_{cell} of µc-Si:H single-junction cells (0.9 µm i-layer thickness) on ZnO:Al front contacts shown in Fig. 2.

Fig. 4: Cell current density j_{QE} determined employing quantum efficiency measurements (left axis) and calculated normalized aperture-area module efficiencies (right axis, employing w_a = 5 mm) as function of front-contact carrier concentration. Nominally identical TCO films were used for the solar-cell evaluation. Cell current density of the treated and untreated half of the same sample are plotted by the same symbol shape. The full line represents a calculated cubic fit. Dotted and dashed lines represent calculations based on this fit employing $w_a = w_{a,opt}$ and w_a = 5 mm, respectively. The normalization of aperture-area efficiency was done with respect to the average value of reference-cell calculations.

Fig. 5: Results of the TDC-variation series as a function of the substrate temperature. The carrier concentration N (Fig. 5a) and the TCO thin-film resistivity ρ (Fig. 5b) determined by Hall measurements, as well as cell current density j_{QE} (Fig. 5c) of µc-Si:H single-junction solar cells (i-layer thickness 1µm) are shown. For comparison, the range of property variation that was observed by vacuum annealing is indicated by dashed horizontal lines.

Figures

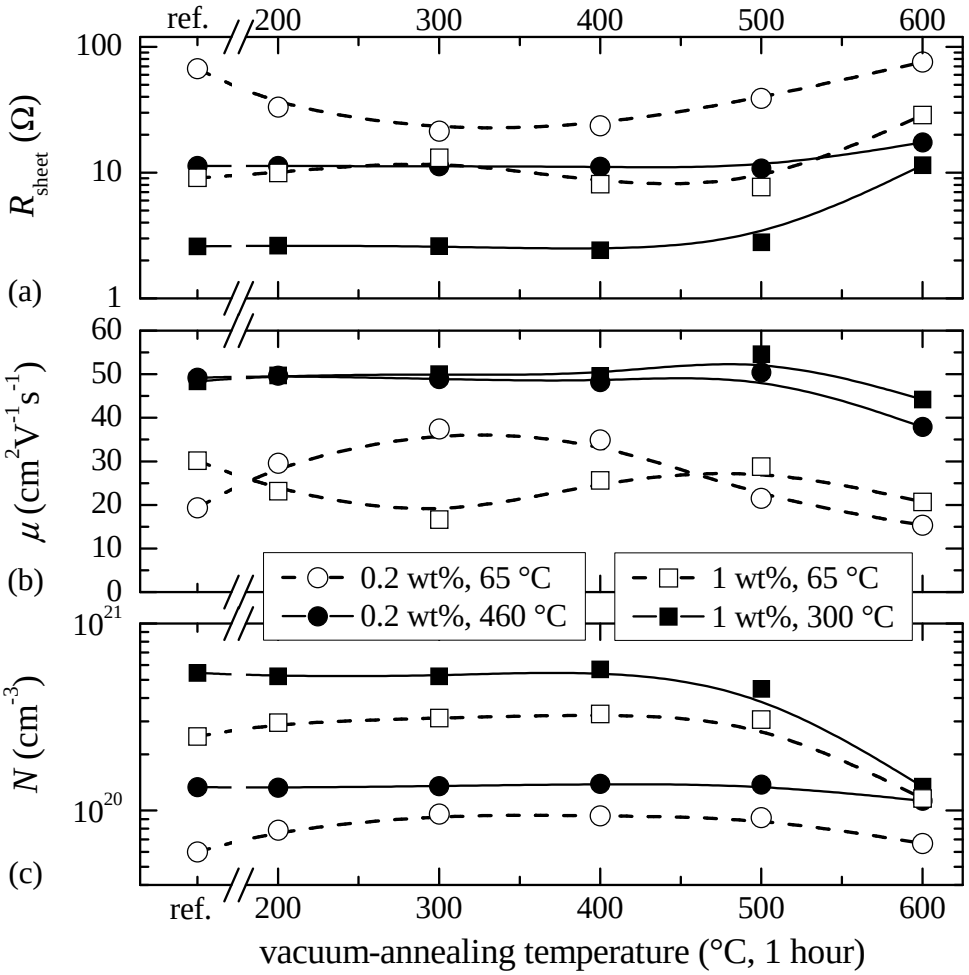

Fig. 1

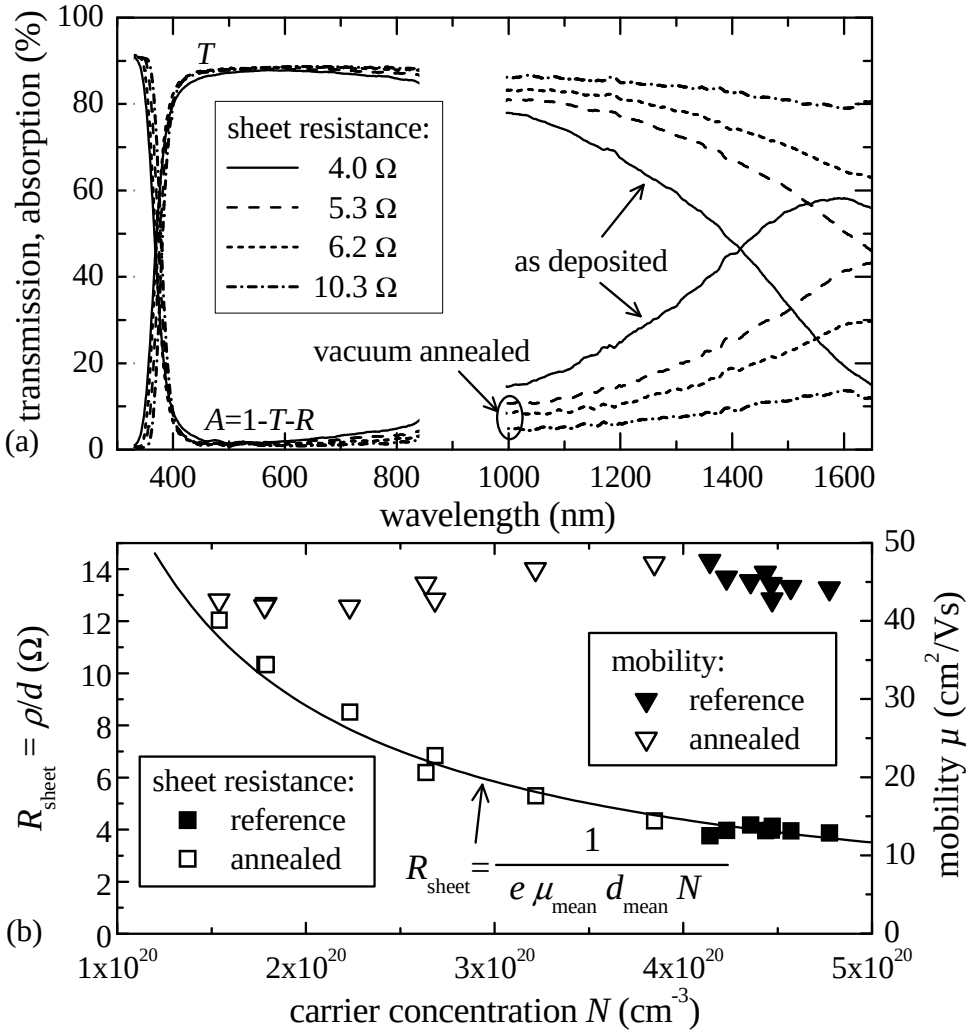
(a)
transmission, absorption (%)
T
A=1-T-R
sheet resistance:
4.0 Ω
5.3 Ω
6.2 Ω
10.3 Ω
as deposited
vacuum annealed
wavelength (nm)
(b)
$R_{sheet} = \rho/d$ (Ω)
mobility μ (cm^2/Vs)
sheet resistance:
reference
annealed
mobility:
reference
annealed
$R_{sheet} = \frac{1}{e\,\mu_{mean}\,d_{mean}\,N}$
carrier concentration N (cm^{-3})

Fig. 2

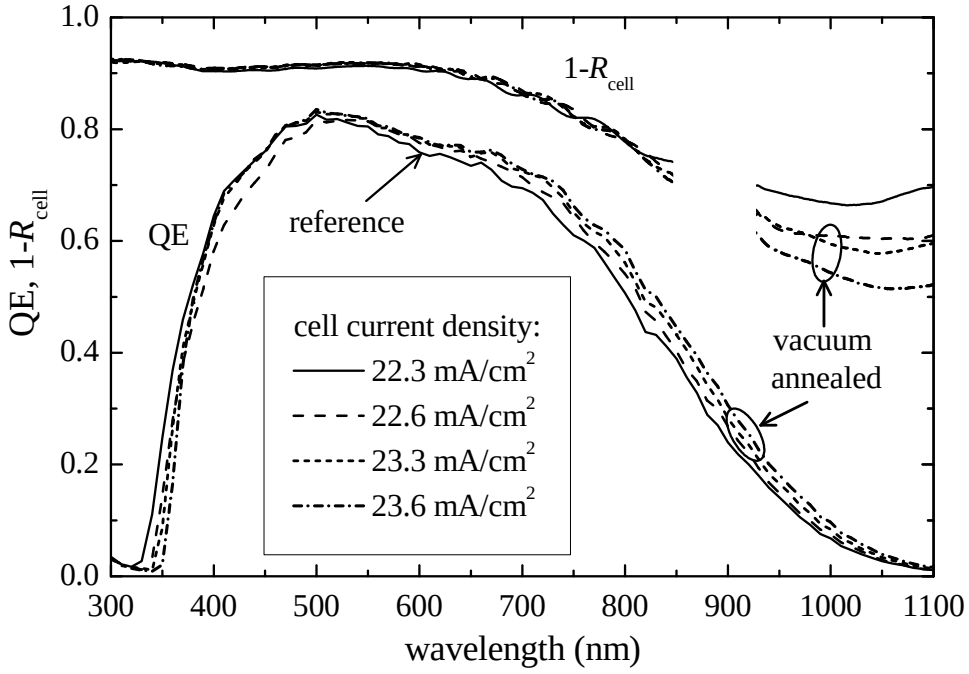
1.0
0.8
0.6
0.4
0.2
0.0
QE, 1-R_{cell}
1-R_{cell}
QE
reference
cell current density:
22.3 mA/cm^2
22.6 mA/cm^2
23.3 mA/cm^2
23.6 mA/cm^2
vacuum
annealed
300
400
500
600
700
800
900
1000
1100
wavelength (nm)

Fig. 3

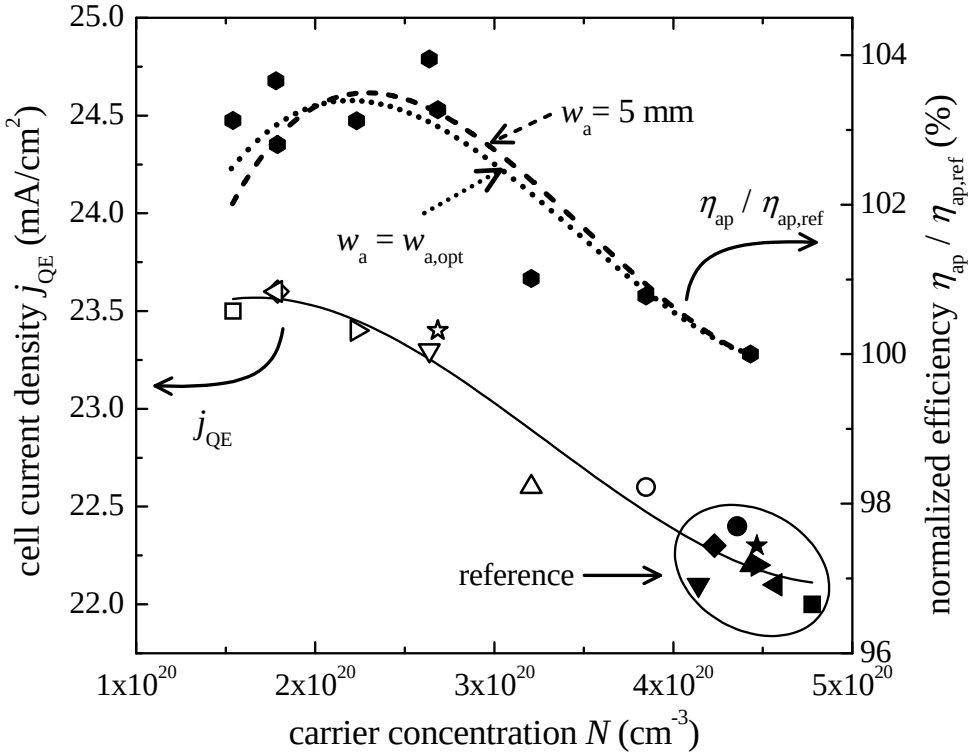
25.0
24.5
24.0
23.5
23.0
22.5
22.0
cell current density j_{QE} (mA/cm^2)
104
102
100
98
96
normalized efficiency η_{ap} / $\eta_{ap,ref}$ (%)
w_a = 5 mm
w_a = $w_{a,opt}$
η_{ap} / $\eta_{ap,ref}$
j_{QE}
reference
1x10^{20}
2x10^{20}
3x10^{20}
4x10^{20}
5x10^{20}
carrier concentration N (cm^{-3})

Fig. 4

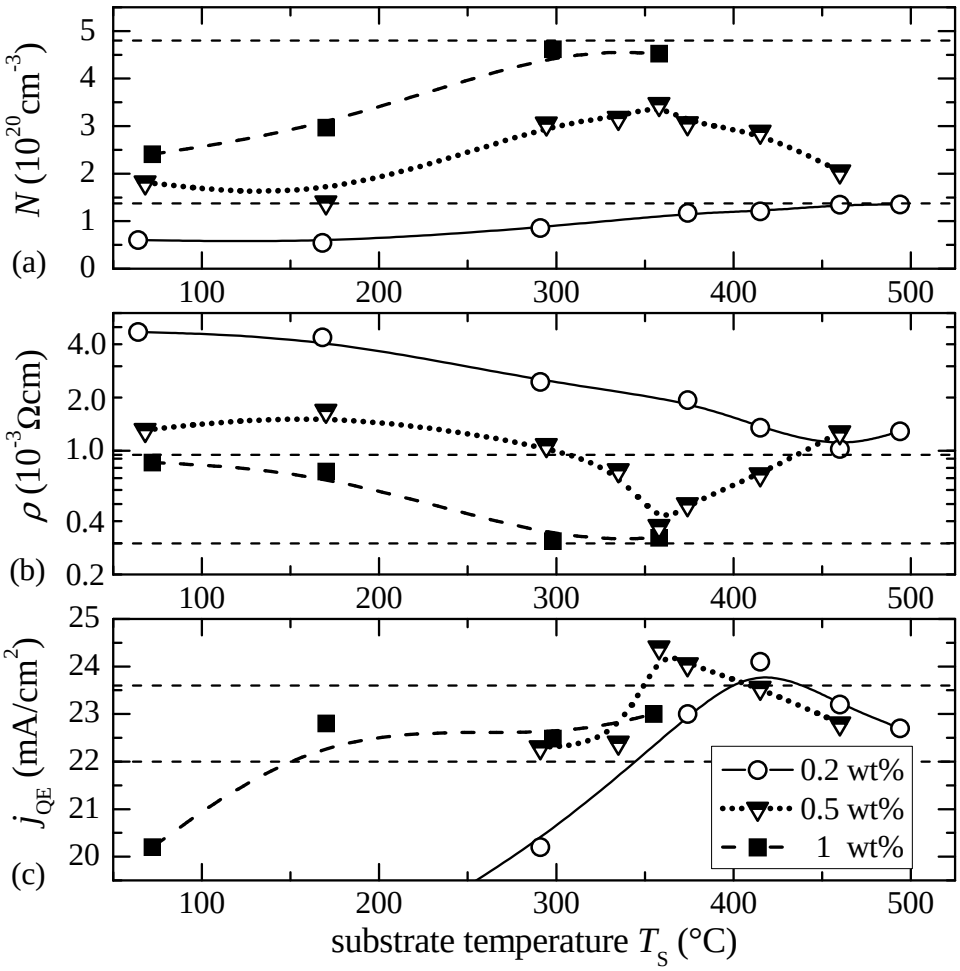
(a)
N (10^{20}cm^{-3})
(b)
ρ (10^{-3}Ωcm)
(c)
j_{QE} (mA/cm^2)
0.2 wt%
0.5 wt%
1 wt%
substrate temperature T_S (°C)

Fig. 5